Extensive sorption of Amoxicillin by highly efficient carbon-based adsorbent from palm kernel: Artificial neural network modeling

Khadijeh Jafari [a], Mohsen Heidari [b], Ali Fatehizadeh [a,c], Kavoos Dindarloo [d], Vali Alipour [d], Omid Rahmanian [d,*]

[a] Environment Research Center, Research Institute for Primordial Prevention of Non-Communicable Disease, Isfahan University of Medical Sciences, Isfahan, Iran
[b] Department of Environmental Health Engineering, Faculty of Medical Sciences, Tarbiat Modares University, Tehran, Iran
[c] Department of Environmental Health Engineering, School of Health, Isfahan University of Medical Sciences, Isfahan, Iran
[d] Department of Environmental Health Engineering, Faculty of Health, Hormozgan University of Medical Sciences, Bandar Abbas, Iran

A B S T R A C T

In the present study, a new sorbent was fabricated from Palm kernel (PK) by dry thermochemical activation with NaOH and characterized by FTIR, X-ray diffraction, FE-SEM and BET, which was used for the Amoxicillin (AMX) sorption from aqueous solution. The influence of effective parameters such as pH, reaction time, adsorbent dosage, AMX concentration and ionic strength on the sorption efficacy of AMX removal were evaluated. The main functional groups on the surface of the magnetic activated carbon of Palm Kernel (MA-PK) were C–C, C–O, C=O and hydroxyl groups. The specific surface of char, activated carbon Palm Kernel (AC-PK) and MA-PK were 4.3, 1648.8 and 1852.4 m^2/g, respectively. The highest sorption of AMX (400 mg/L) was obtained by using 1 g/L of sorbent at solution pH of 5 after 60 min contact time, which corresponding to 98.77%. Non-linear and linear models of isotherms and kinetics models were studied. The data fitted well with Hill isotherm ($R^2 = 0.987$) and calculated maximum sorption capacity were 719.07 and 512.27 mg/g from Hill and Langmuir, respectively. A study of kinetics shows that the adsorption of AMX follows the Elovich model with $R^2 = 0.9998$. Based on the artificial neural network (ANN) modeling, the MA-PK dosage and contact time showed the most important parameters in the removal of AMX with relative importance of 36.5 and 25.7%, respectively. Lastly, the fabricated MA-PK was successfully used to remove the AMX from hospital wastewater.

1. Introduction

In recent decades, the occurrence of emerging environmental pollutants has been seriously considered. Pharmaceutical products are one of the main groups of emerging pollutants [1–3]. Among pharmaceutical compounds, antibiotics are extensively applicable to humans, animals and plants [4,5]. Among pharmaceutical products, AMX products have had the highest consumption. AMX is a semi-synthetic group of beta-lactam that is used against both gram-negative and gram-positive bacteria in wide range [6,7]. AMX is used as a medicine for human and veterinary applications and should be considered due to its high consumption in the world and Iran as well [4,8–10]. The release of AMX into the environment can lead to chronic dangers [11–13]. In order to remove antibiotics from

* Corresponding author.
  E-mail addresses: om.rahmanian@gmail.com, omid.rahmanian@hums.ac.ir (O. Rahmanian).

wastewater and water, different methods are used, including advanced oxidation, adsorption, coagulation, flocculation, sedimentation, filtration, membrane processes, biological processes and combination processes [5,6,14–21]. Since the removal efficiency is low in biodegradation methods using antibiotics as a toxic substance for purifying organisms. Advanced oxidation methods, in addition to its high cost, often result in its degradation and mineralization, which causes secondary problems. Among physical, biological and chemical methods [22–24], physical removal is the most efficient process that is used for pharmaceutical wastewater treatment. In order to easy operation, low cost, and lack of toxic by-products, adsorption methods have been developed as an appropriate and applied method [25–27]. Activated carbon, among surface adsorbents, due to high adsorption capacity, high porosity and specific surface is most used to remove the organic compounds from contaminated aqueous solution [4,28].

Increasing the area of adsorption specific surface that can be achieved by applying corrective methods such as loading nanoparticles on the activated carbon surface is one of the efficient factors for increasing the removal yielding adsorption methods [29–31]. Among the nanoscale materials that have shown good efficiencies in wastewater and water treatment, some examples can be mentioned, such as membrane filters, zeolites, carbon compounds, metal oxides, metal nanoparticles, etc. [32–34].

The preparation of carbon-based bio-adsorbent from PK, which is abundant in the southern regions of Iran as a solid waste, especially in the Fars and Hormozgan provinces, was the novelty of this study. Also, the novel bio-adsorbent is used to AMX removal from aqueous solution and hospital wastewater in order to evaluate the capability of the prepared adsorbent. The factors that affect the AMX removal with adsorption reaction such as contact time, pH, dosage of adsorbent, AMX concentration, isotherm and kinetics of adsorption reaction were examined as well. Moreover, ANN modeling was carried out to compare the results of experimental analysis and the predicted state to determine the percentage contribution of each variable in the process and also verify the results obtained with the predicted state.

2. Experiments

2.1. Materials and methods

All chemicals such as $FeCl_2.4H_2O$ ($\geq$99%), $FeCl_3$ ($\geq$98%), HCl (37%), NaCl ($\geq$99.5%), water and methanol (HPLC grade, 99.9%) were prepared by the Merck. The fresh PK was prepared from Kazeroun city in the Fars province of Iran. AMX ($\geq$99% purity, Farabi Pharmaceutical Company) is prepared from Isfahan (Iran). The solution pH was measured through a digital pH meter (WTW7110, Germany) using NaOH and HCl 0.1 mol/L.

2.2. Producing char from the PK

As previously done by Jafari et al. [35], at ambient temperature the PKs were dried first and then crushed using the mortar. Then the stainless-steel reactors that contained crushed PKs placed undergoing N_2 gas (with a flow rate that was 100 cm^3 per minute) for 2 h at 500 °C (electric furnace: 5 L, 220 V, 2000 W and 50–60 Hz). The produced char was again grounded and sieved to make particles to the size of about 400–500 μm.

2.3. Activated carbon production (AC-PK)

For obtaining the activated carbon, char and dry NaOH were blended in a 1:3 ratio [36]. The mixed char and NaOH was then poured into a reactor (stainless steel) in the furnace (electrical) and the mixed material was subjected to horizontally gas of N_2 (100 cm^3/min as a flow rate) at 700 °C for 1.5 h. In the second step, after cooling, the reactor was eliminated from the furnace, then, AC from PK was washed by deionized water. In the next step, with a cellulose membrane filter (0.45 μm) and vacuum pump, the activated carbon was washed and the chemical impurities were removed using 0.1 mol/L HCl. The washing phase was applied to neutralize the residue using deionized water several times. Then, the AC powder was dried for 24 h at 110 °C in a digital sterilizer.

2.4. Synthesis of Fe_3O_4 particles

The Fe_3O_4 magnetic particles were produced using $FeCl_2.4H_2O$ (1.113 g) and $FeCl_3$ (1.817 g), as previously performed by similar study [37]. Separately, each of the materials was poured into 50 mL deionized water and blended by heater-magnet at 80 °C (alpha D-500). Also, 15 mL of NH_3 (25%) that was purged by nitrogen gas was added (for 30 min) as droplets to the solution. In the next phase, to react the solution, it was allowed for 2 h. The change in the solution color (orange to black) was an indication in the effective creation of Fe_3O_4 magnetic particles. Using an external magnet, the magnetic black Fe_3O_4 nanoparticles were isolated and washed ten times using deionized water and five times using ethyl acetate ($C_4H_8O_2$: 96% purity). Fe_3O_4 nanoparticles at 70 °C were dried in a digital sterilizer for 12 h. The dried Fe_3O_4 nanoparticles were powdered and milled and then separated with a sieve (500 μm). The produced Fe_3O_4 was 1.202 g. The product was kept at a refrigerated temperature and desiccated in polyethylene containers due to its sensitivity to humidity.

2.5. Fabrication of MA-PK

Ethyl alcohol (96%) with a volume of 200 mL was added to 5 g of AC produced by NaOH, to synthesize the MA-PK, and it was exposed to ultrasonic waves in an ultrasonic device that was Digit starsomic 18–35. Moreover, as formerly reported by Bagheri et al.

ethanol (50 mL, 96%) was added to Fe_3O_4 (0.5 g) and for 1 h was placed in an ultrasonic device [37]. Then, the solution of Fe_3O_4 nanoparticle with the mass ratio of 1:10 was added to the AC-ethanolic solution and placed in Digit starsomic 18–35 for 8 min. It was then inserted for about 12 h at 250 rpm in a Shaker with a Heidolph Unimax 1010 model. So, the ethanol aqueous solution was eliminated using a cellulose membrane (0.45 μm) and a vacuum pump. The MA-PK was washed 7 times by deionized water as well as dried for 16 h at 80 °C. Then MA-PK was ground into the form of a powder and stored in the desiccator until the tests were done.

2.6. Instruments

SEM images were created by FE-SEM Tescan Mira II (Czech Republic). The images were used to show the shape, morphology and the size of the adsorbent particle on the surface of the adsorbent after and before activation, and also the MA-PK morphology. By X-ray radiation (anode of Cu kα at a normal angle that is 10–80°, using the Dutch PW1730-XRD device), X-ray diffraction (XRD) spectrometry was conducted. Each sample, indeed a powder with a very fine size, was subjected to X-ray bombardment by the 1.54056 Å for wavelength and the size was designed at 0.05. A diffraction pattern or diffractogram resulted. Each sample had an individual diffraction pattern in which the compound type was identified using databases of XRD and patterns compared with standard patterns of diffraction. In order to determine the unknown quality of the samples, the bonds in the molecules of MA-PK and the kind of functional groups, samples were recognized with the Nicolet Avatar-FTIR ATR for FT-IR analysis. Also, the solution samples were analyzed with BEL SORP mini II-BET, to investigate the area of the adsorbent surface.

2.7. Experiments of AMX sorption

At first, 1000 mg/L of the AMX stock solution was prepared with deionized water in a polyethylene container (almost 60 mL with 25 mL of AMX solution). In a closed environment, all of the experiments of AMX adsorption were carried out for AMX concentrations of 100–1000 mg/L, MA-PK dose of 0.1–3 g/L, at contact times of 5–240 min, and at pH values of pH 2–9. Then, the solution pH was set by NaOH and HCl (0.1 mol per litter). Tests were carried out on the temperature of the room. For mixing the suspension of adsorbent and adsorbate, samples were put on a shaker (250 rpm). After a different reaction time, samples were filtered with syringe Cellulose filters (0.45 μm). With a HPLC (Shimadzu) instrument, a calibration curve plotted by UV detector (at 230 nm). The AMX concentration was calculated by injecting samples into HPLC. The reverse HPLC phase column was ODS (octadecyl silane) with dimensions of 250×4.6 mm by volumes of 20 μL injections. Also, the mobile phase involved water and methanol (60:40 ratio). Also, each step of the test was repeated 2 times, then, the average of the data was considered as the final result. Using the following relationships (Equations of (1, 2)), the AMX content that adsorbed (mg) on the MA-PK and then removal efficiency of contaminant was found:

$$q_e = \frac{C_0 - C_e}{m} \times v \tag{1}$$

$$\% \text{ Removal efficiency} = \left(\frac{C_0 - C_e}{C_e}\right) \times 100 \tag{2}$$

where q_e is the adsorption capacity under equilibrium conditions (mg/g). C_0 and C_e are the initial and equilibrium concentrations of AMX (mg/L), respectively. Moreover, v and m are the solution volume (L) and the adsorbent mass (g), respectively.

Fig. 1 represents the chromatogram of the AMX after injecting into HPLC. According to the calibration curve, the amount of AMX standards that were obtained after injecting into HPLC had a regression coefficient of 0.9991 and a wide linear dynamic range. The calibration curve equation was $y = 61105 \times - 5133$ (where the peak area is y and the AMX concentration is x).

2.8. Kinetic and isotherm models

In this study, the experimental adsorption data were fitted to the kinetic and isotherm models in order to further characterize the adsorption phenomenon. In Table 1, the equations of kinetic and isotherm models are shown. The original forms of kinetic and isotherm models were fitted non-linearly to the experimental adsorption data using Origin Lab Pro (2022) software, while the linear kinetic of intraparticle diffusion (IPD) model was evaluated. The kinetic study was done by considering the experimental data of adsorption rates at different reaction times. In this study, four kinetic models, including pseudo-first-order, pseudo-second order, Elovich, and IPD were considered.

The basis of the pseudo-first-order model is that the adsorption process occurs through controls on a boundary layer, while the pseudo-second-order kinetic shows that the chemical adsorption is predominant and controls the adsorption mechanism [38,39]. The Elovich kinetic describes the adsorption process as a group of reaction mechanisms, such as surface diffusion, active catalytic surfaces and adsorption onto the active site of adsorbent [40]. In this model, the energy of the adsorbent surface is heterogeneously distributed and the adsorption kinetics, in low surface coverage, is not affected by the interaction or repulsion between the molecules of the adsorbent surface [41]. The kinetic of IPD examines the mass transfer of adsorbed molecules from the bulk solution to the external surface of the adsorbent, the mass transfer of the adsorbed material to the internal surface of the adsorbent and finally, their absorption on the active sites of the adsorbent [42]. In this model, three linear regions are drawn for each stage of the absorption process [43]. The first linear region starting from the origin represents the transfer of AMX molecules from the bulk liquid to the external surface of MA-PK. The second linear region corresponds to the entry of AMX molecules into the porous structure of MA-PK or IPD. Finally, the
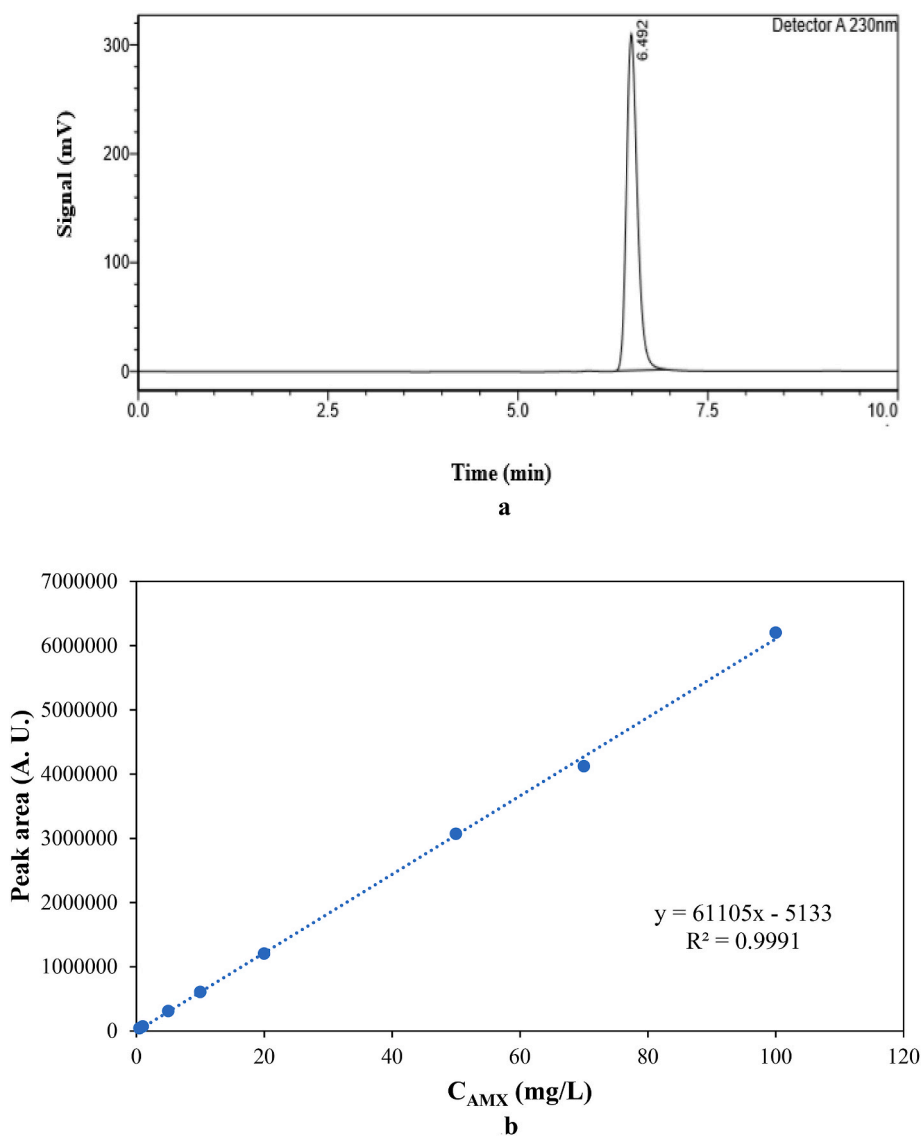
Fig. 1. a) A chromatogram obtained from standard AMX injection ($C_{AMX. ST}$ = 50 mg/L) and b) the calibration curve of AMX ($C_{AMX.ST}$ = 0.5–100 mg/L).

third linear region shows the equilibrium phase of the adsorption process [44]. The IPD was used to determine which part of diffusion is rate controlling [43].

The Langmuir adsorption model expresses monolayer, homogenous, and uniform adsorption on surfaces with equal energy on all surfaces of adsorbent. In the Langmuir isotherm, all adsorption sites are identical to those of the adsorbing molecules [35]. The Freundlich isotherm expresses a multi-layered, heterogeneous, and non-uniform adsorption on the surface of adsorbent [45]. The isotherm of Temkin is a newer model of equilibrium isotherms which describes the indirect adsorption effects and adsorbing interactions on isotherm of adsorption [46,47]. Temkin assumes that the adsorption heat for all of the adsorbed molecules is reduced linearly by the increase of the adsorbent surface coverage [48]. Dubinin-Radushkevich isotherm is used to determine the thermodynamic parameters of the adsorption process based on the adsorption of heterogeneous surfaces [49–51]. The Redlich-Peterson model considers both monolayer and multilayer adsorption mechanisms. The exponent (g) in this model is between 0 and 1. If the g value equals 1, the Redlich-Peterson equation works like Henry's law. For g < 1, and a_{RP} and b_{RP} > 1, the Redlich-Peterson adsorption isotherm will tend to the Freundlich model. It is worth mentioning that if the power of g goes to number 1, Redlich-Peterson isotherm works like Langmuir isotherm [43]. The Hill isotherm model is a cooperative phenomenon in which a ligand binds to a site on a macromolecule. In this case, different binding sites on a macromolecule may be affected. Q_H is the Hill isotherm adsorption capacity, n_H is the Hill bond interaction coefficient, and K_H is the Hill constant [52].

Table 1
Equations related to the calculation of kinetic models and reaction isotherms.

Kinetic models	Intraparticle diffusion	$q_t = k_{id}\sqrt{t}\,C_i$; or $q_t = k_b t^{0.5} + C$
	Elovich	$q_t = \dfrac{1}{\beta}\ln(1 + \alpha\beta t)$
	Pseudo-first order	$q_t = q_e(1 - e^{-k_1 t})$; $h_0 = k_1 q_e$
	Pseudo-second order	$q_t = \dfrac{k_2 q_e^2 t}{1 + k_2 q_e t}$; $h_0 = k_2 q_e^2$
Isotherm models	Hill	$q_e = \dfrac{q_H\,C_e^{n_H}}{k_H + C_e^{n_H}}$
	Temkin	$q_e = \dfrac{RT}{b_T}\ln(k_t C_e)$
	Freundlich	$q_e = k_F C_e^{1/n_f}$
	Langmuir	$q_e = \dfrac{q_m\,k_L\,C_e}{1 + k_L\,C_e}$; $R_L = \dfrac{1}{1 + k_L\,C_0}$
	Redlich-Peterson	$q_e = \dfrac{a_{RP}\,C_e}{1 + b_{RP}\,C_e^{g}}$
	Dubinin-Radushkevich	$q_e = q_s e^{-\beta\varepsilon^2}$

The pseudo-first order and pseudo-second order constants = k_1 and k_2, respectively; the Elovich constants = α and β; IPD constants are the k_{id} and C_i; Freundlich constants are the k_F and n_f; maximum monolayer adsorption capacity is q_m; k_L is the Langmuir constant and R_L is the Langmuir separation factor; Redlich-Peterson constants are the a_{RP}, b_{RP} and g; variation of the adsorption energy in Temkin model shown by b_T and k_T is the Temkin constant; universal gas constant is the R (8.314 j/mol °K) as well as T is the absolute temperature (°K).

2.9. ANN modeling

Artificial neural network model is a method that is used in order to model the complex processes [53,54]. ANN, in which the neurons are the processing units, has been carried out successfully for modeling of water treatment processes [55,56]. ANN consists of 3 main neurons layers that are called output, input and hidden layers. The neurons nodes in each layer, layers, and the transfer functions among layers form the topology of the network [57,58]. All ANN evaluation was performed by Matlab 7 with ANN toolbox. Also, in the present study, adsorption of AMX on MA-PK was modeled through a 3-layered feed-forward back diffusion neural network by linear transfer functions. A total of 40 experimental runs were used in order to feed the structure of an artificial neural network. Then, the data sets were separated into validation, subset of tests, and training that included 36th, 38th, and 40th samples, respectively. In order to validate the calculation and modeling net power, the test sets and validation were randomly chosen from the experimental data. The variables ranges are shown in Table 2. Training the artificial neural network is sentient to the neuron's nodes in the hidden layer. So, a series of topologies in which the number of neurons in their hidden layer (2–20 neurons layers) were used due to model the AMX removal process on the MA-PK. MSE (Mean squared error) was used to assay the number of neurons effect on ANN validity (Equation (3)) [59,60]:

$$MSE = \left(\sum_{i=1}^{N} \left| \left(R_{i,pre} - R_{i,exp} \right) \right|^2 \right) \bigg/ N \qquad (3)$$

in this equation, N is the data point number, $R_{i,\,exp}$ and $R_{i,\,pre}$ are network experimental and prediction efficiency of AMX removal, respectively. also, i is a data index.

Table 2
Input and output parameters and their ranges.

Variables	Ranges
Input layers	
pH	2–9
AMX concentration (mg/L)	100–1000
MA-PK dose (mg/L)	0.1–3
Time (min)	5–240
NaCl concentration (mg/L)	0.1–5
Output layers	
AMX removal efficiency (%)	13.22–96.74

3. Results and discussion

3.1. MA-PK characteristics

Fe_3O_4 particles were used for magnetizing activated carbon obtained from the PK. Iron oxides for activation should be fixed on the surface of AC-PK so that X-ray diffraction was used to show the magnetic activated carbon-crystalline structure [61]. The XRD patterns of magnetized nanoparticles (Fig. 2) confirmed the Fe_3O_4 crystals on the surface of adsorbent using adsorbent XRD patterns by applying Cu Ka by 10–80° as a normal radiation angle. Based on the results, Fe_3O_4 sample peaks at 2Θ° of 30.34, 35.57, 43.41, 53.76, 57.13 and 62.95, are quite consistent with the Fe_3O_4 standard XRD spectrum, meaning that other iron compounds do not precipitate on the activated carbon surface [62]. In terms of the crystalline structure and particle size, according to the shape, this indicates that the wide range and weak peaks in the sample are different, thus the particle size on the adsorbent surface and the average crystal size are small. Failure to observe other compounds in the prototype of the standard XRD model of the nanoparticle can be referred to as the other amorphous compounds (other non-crystalline compounds) or their small amount of them in the sample. The peak angle of 35.57° has the highest intensity that the spacing between the plates is 2.52 Å. Also, the FWHM (full width at half maximum) is 0.59°.

FTIR analysis identifies different adsorbent groups and functional groups. To recognize the original functional groups available on the adsorbent surface, the quality of the unknown samples and their contributions to the adsorbent molecules using Nicolet Avatar-FTIR-FTIR ATR were calculated. As shown in Fig. 3, the adsorption band is shown for char, activated carbon and MA-PK. The adsorption peak of about 1600–1750 cm^{-1} is relevant to aromatic compounds of C–C, which found in all of the three samples. The adsorption peak of about 3400 cm^{-1} is relevant to the $°OH$ (hydroxyl) tensile strength or water molecules, which is much higher in active carbon and MA-PK samples than in the char sample. Also, the high levels of the C–O and aromatic rings in the adsorption peak were formed at 1054 to 1226 cm^{-1} after activation, which is higher in the magnetized adsorbent than activated carbon and char. The adsorption peak shows C=O groups at 1700 cm^{-1}, which are more composed in the activated carbon and MA-PK samples. The adsorption peak of about 2885–2955 cm^{-1} is associated with the functional groups Methylene and Methyl.
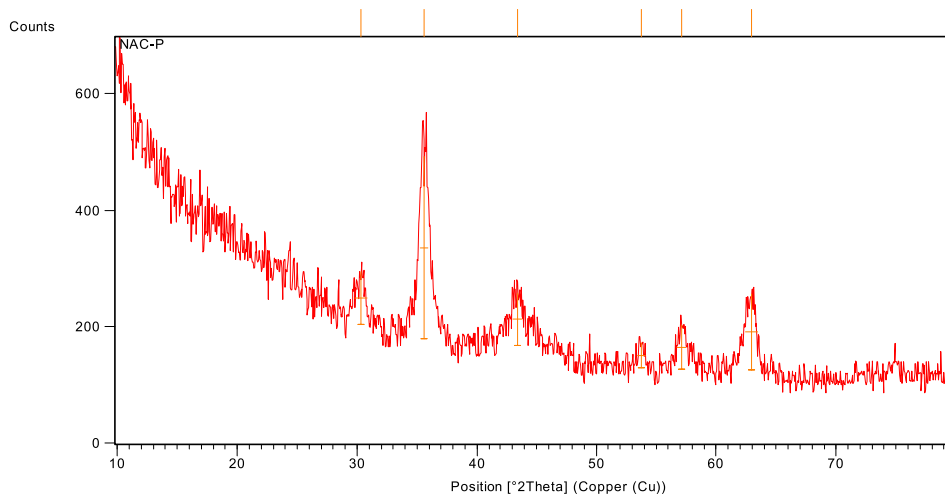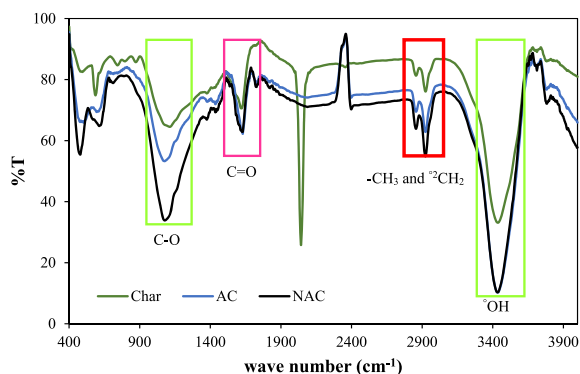

Fig. 2. The XRD patterns of MA-PK

Fig. 3. FTIR spectra of char, activated carbon and MA-PK.

The shape and adsorbent surface morphology were evaluated using FESEM before and after the activation of the material by NaOH and also after the production of the magnetic particles as well [43]. Regarding Fig. 4 a-c, the surface of the char sample, according to the volatile compounds released during the carbonized time period of PK, has a rugged surface, and the rate of degradation and formation of absorption pores is poor and insignificant. In Fig. 4b, the adsorption level is clearly shown in the activation phase in comparison to the primary production stage, the activated carbon production, and after loading of the Fe_3O_4 magnetic particles on the activated carbon. Sodium hydroxide is known to be an active agent for premature carbonaceous substances. The development of cavities using NaOH is accompanied by reduction and oxidative modification in order to isolate and degrade the graphite layers. Therefore, some possible reactions between the carbon and active intermediates cause the formation of CO_2, H_2 and CO that develops the porosity of the surface. Adsorption cavities created on the adsorbent surface are a good place to penetrate the molecule of AMX into the structure of carbon, allowing disposal of mesoporous and microporous adsorbents and interactions between surface functional groups [63]. In addition, the size of nanoparticle crystals on the adsorbent surface in these figures was about 36 nm.

The distribution of pore size and specific adsorption surface using the BET system was determined according to the measured amount of N_2 gas adsorbed and desorbed with the material surface at 77 K as a constant temperature of nitrogen [64]. The specific surfaces of char, AC-PK and MA-PK were 4.3, 1648.8 and 1852.4 m^2/g, respectively. According to the results, the absorbance pore volume increased after activation. Also, after loading magnetic particles on the AC-PK surface, the amount of special adsorption area and adsorption cavities on the MA-PK surface were increased.

3.2. pH_{pzc}

The pH_{pzc} indicates a pH at which the charge of the surface is zero. The charge of the adsorbent surface is negative ($-$) at pH higher than pH_{pzc}, and the adsorbent charge of the surface is positive ($+$) at pH $<$ pH_{pzc} [65]. To determine pH_{pzc}, 50 mL of sodium chloride 0.1 mol/L was poured into a 100 mL container. The pH of the solutions was adjusted using Sodium hydroxide and Hydrochloric acid 0.1 mol/L, in the pH range of 2–9. Afterwards, 0.15 g of MA-PK was added to each sample container and after 48 h, the pH of solutions was measured again. pH_{pzc} is equal to the pH value obtained by initial pH (pH_i) and final pH (pH_f). The pH_{pzc} in this study was to be 6.42.

3.3. Effect of solution pH

pH is one of the main factors that should be considered in adsorption processes because of the effect on the charge of the adsorbent surface and the pollutants ionization. In order to determine the pH effect, a solution of 400 mg/L of AMX at pH of 2–9 was adjusted using Sodium hydroxide and Hydrochloric acid 0.1 mol/L. The MA-PK effects on the solution pH and AMX removal can be described
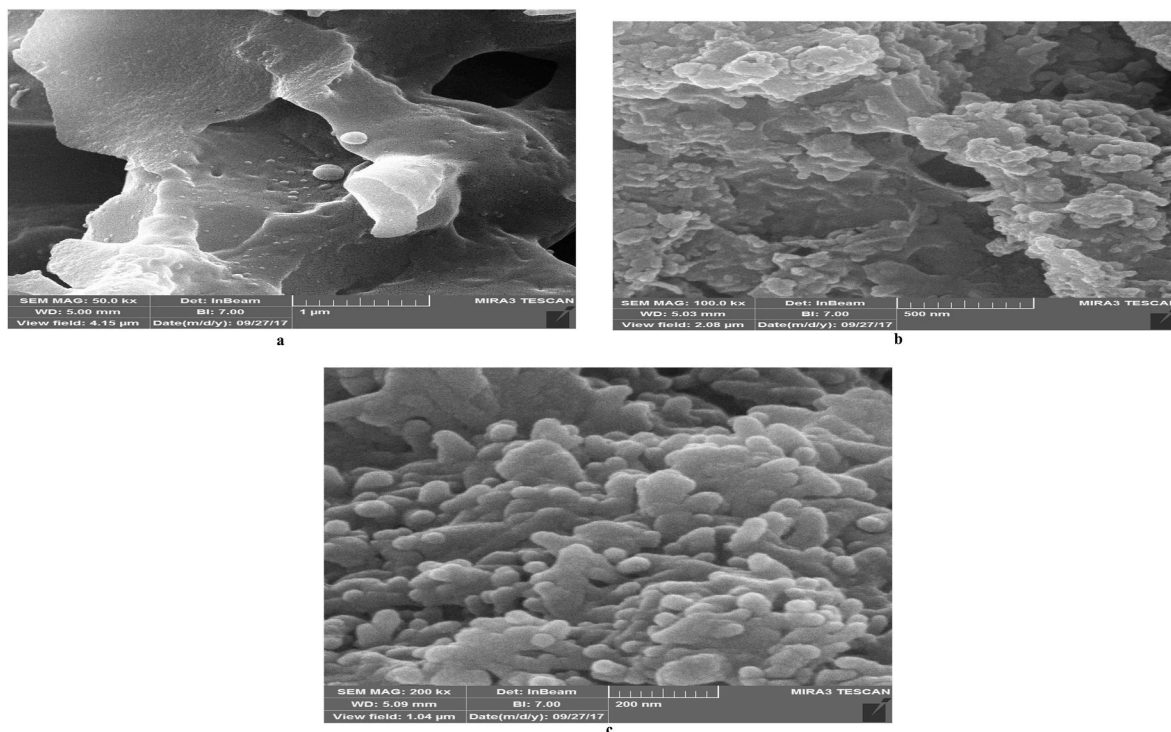

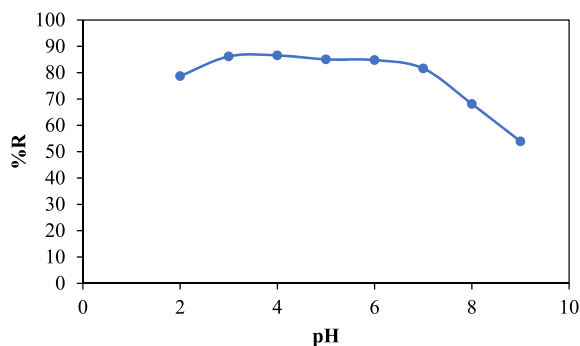**Fig. 4.** FESEM images for a) char b) activated carbon and c) MA-PK.

Fig. 5. The effect of pH on AMX adsorption by MA-PK (time = 120 min, C_{AMX} = 400 mg/L, adsorbent dose = 1 g/L, rpm = 250).

with respect to the pk$_a$ of AMX and the charge of adsorption surface. The degree of dissociation depends on the pK$_a$ of AMX (pK$_a$ of 2.4, 7.4 and 9.6 for carboxylic acid, amines and phenols, respectively). So, pH determines the condition of ionization for AMX molecules in the solution phase which depends on the values of pH. Regarding the pK$_a$ carboxylic acid functional groups of AMX and pH$_{pzc}$ (pH$_{pzc}$ = 6.42), at pH of 5 the charge of AMX and surface charge of adsorbent are negative and positive, respectively. The isoelectric point of AMX is 5.2. According to Fig. 5, the AMX molecules are adsorbed on the adsorbent by electrostatic reactions. So, it can be said that the dominant mechanism for adsorption in the aqueous solution has been related to electrostatic reactions.

According to Fig. 5, since the changes in the RE of AMX were negligible because of the change of the pH from 3 to 6, it can be stated that the pH factor has no considerable effect on the AMX removal in this range and has little effect. For further experiments, pH = 5 was considered as optimal.

3.4. Influence of contact time

Due to enhancement of the removal efficiency of the MA-PK, reaction time is the main parameter to determine the optimum time for the adsorption of AMX onto MA-PK (400 mg/L for concentration of AMX, absorbent dose of 1 g/L and pH = 5). Experiments were carried out at different interval times of 5–240 min. In the first 60 min, the AMX removal efficiency rapidly increased, probably due to the availability of adsorption cavities on the MA-PK surface. According to Fig. 6, the adsorption rate was not changed significantly after 60 min and therefore, this time was selected as the optimal time.

3.5. Effect of MA-PK dose

It is advisable to use an optimal dosage of adsorbent in order to prevent excessive adsorbent usage. The MA-PK dose effect on the efficiency of AMX removal at different doses of adsorbent (0.1–3.0 g/L) was investigated and presented in Fig. 7. In this study, with increasing the dose of MA-PK (0.5–3 g/L), the removal efficiency was increased from 52.2 to 98.8%, but the adsorption capacity (q) diminished from 417.3 to 131.7 mg/g. It may be due to the agglomeration of adsorbent in high-doses that may decrease the available surface area and increase the length of the propagation pathway [66]. Increasing adsorption efficiency can be due to the general increase in the adsorbent surface areas, including the increase in the number of active sites for adsorption reactions [67].
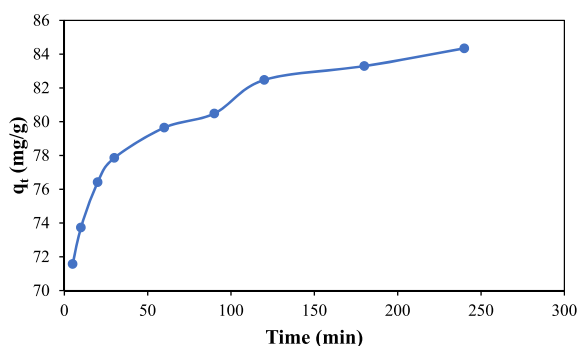

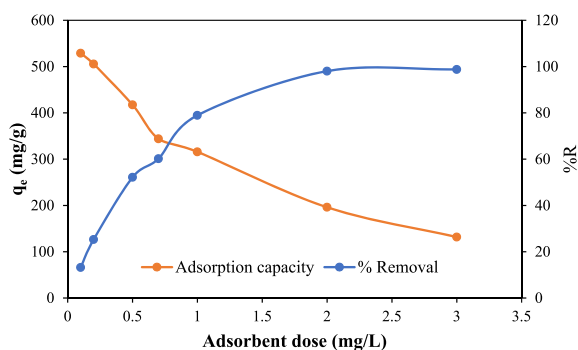**Fig. 6.** Eeffect of contact time (pH = 5, C_{AMX} = 400 mg/L, adsorbent dose = 1 g/L, rpm = 250).

Fig. 7. Effect of adsorbent dose (time = 60 min, pH = 5, C_{AMX} = 400 mg/L, rpm = 250).

3.6. Effect of ionic strength

The ionic strength effect on the adsorption capacity and adsorbent efficiency was measured by NaCl with a concentration of 0.1–5 g/L for AMX removal. The Na^+ ions in the salt compete for active cation exchanger sites in MA-PK. In general, the effect of ionic strength in increasing the efficiency was insignificant (1–2%) and in some cases caused reduced AMX removal efficiency (Fig. 8).

The ionic strength of a sample solution may affect the interactions among species of contaminant and adsorbent [68,69]. A study on the Cefixime adsorption onto KOH- and NaOH-prepared activated carbon showed <3% decrease in the removal efficiency in solutions containing up to 0.7 mol/L NaCl. Altogether, the Cefixime adsorption on the 2 sorbents is not affected significantly by the concentration of NaCl under the applied condition in the present research conditions, which is similar to our study.

3.7. Kinetic study

The kinetics of adsorption was studied to determine the mechanism of the adsorption process (penetration and/or interaction between adsorbate and adsorbent surface) and to determine the factors affecting the adsorption rate [70,71]. Fig. 9 (a, b) determines the kinetic models of adsorption and the results of the absorption kinetics and the summarized results are shown in Table 3. Very low values of β and very high values of α, especially at pH = 5, indicate proper interaction between MA-PK and AMX molecules. The very high value of α (2.11E+09 mg/g.min) is indicative of a very high initial adsorption rate. As can be seen, the reaction kinetics in the present study followed the Elovich model with R^2 equal to 0.9998, indicating that chemical adsorption was the dominant phenomenon (Fig. 9a). The results of Kyzas et al. (2022), show that, among IPD, pseudo-first order and Elovich models, pseudo-second order was the best model according to correlation coefficient (R^2 = 0.998 for 10 mg/L of Benzene) [44]. Similar to our study, the removal of Tetracycline by FONP-PAC followed the Elovich kinetic model with R^2 = 0.996 [40]. Also, the removal of fluoroquinolones and ibuprofen is followed by the Elovich model [41,72]. For pseudo-first-order and pseudo-second-order kinetic models, R^2 was 0.985 and 0.995, respectively. Also, K_{PFO} and K_{PSO} were 0.42 (1/min) and 0.0137 (g/mg.min), respectively.

In the IPD model, the C_i (intercept value) of the plots shows the boundary layer thickness. The rank order of C_i values was C_1 (0) < C_2 (71.46) < C_3 (77.93) (Table 3), showing the lower external diffusion resistance at the first stage of the adsorption process rather than the other two stages, probably due to the availability of more vacant MA-PK adsorption sites. k_{id}, determine the adsorption rate of AMX. According to Table 3, the k_{id} value for the first stage of AMX adsorption at pH = 5 was 32.01 mg/g min$^{0.5}$ which was higher than the other two stages [43]. In Kyzas et al. (2022) study, limiting step, mechanism and controlling the process of ion exchange were done with IPD model. Similar to this study the first stage showed the steepest slope, probably due to the stirring of the adsorption suspension
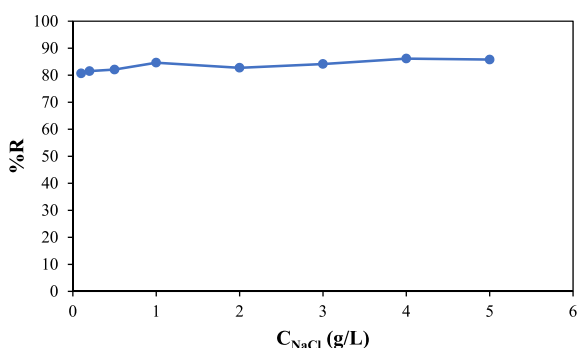

Fig. 8. Effect of ionic strength on the adsorption process (time = 60 min, pH = 5, C_{AMX} = 400 mg/L, adsorbent dose = 1 g/L, rpm = 250 rpm).
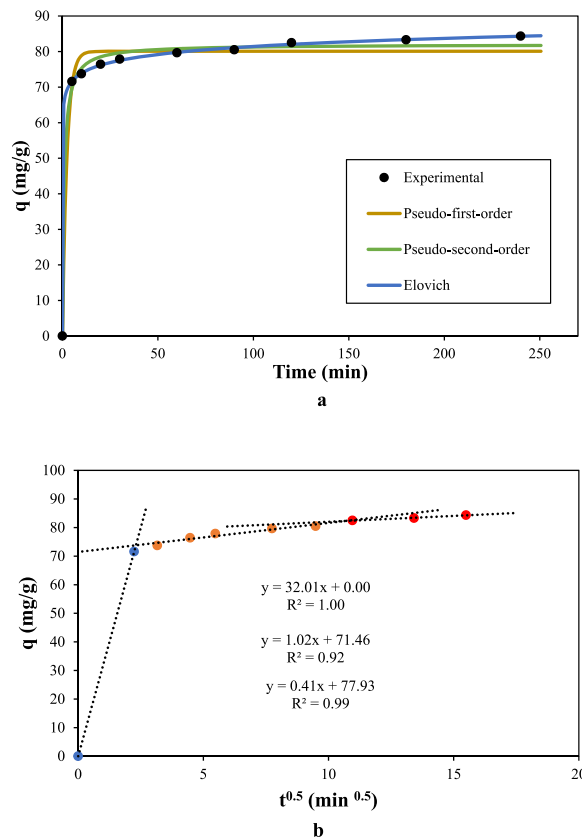
Fig. 9. The non-linear model of a) pseudo-first order, pseudo-second order and Elovich kinetics b) Linear IDP model for AMX uptake onto MA-PK.

Table 3
Results obtained from the kinetics of AMX adsorption onto MA-PK.

Kinetic models	pH = 5	
Intraparticle diffusion	Stage 1	
	$K_{id, 1}$ (mg/g. min$^{0.5}$)	32.01
	$C_{i,1}$ (mg/g)	0
	Stage 2	
	$K_{id, 2}$ (mg/g. min$^{0.5}$)	1.02
	$C_{i,2}$ (mg/g)	71.46
	Stage 3	
	$K_{id, 3}$ (mg/g. min$^{0.5}$)	0.41
	$C_{i,3}$ (mg/g)	77.93
Elovich	β (g/mg)	0.3056
	α (mg/g.min)	2.11E+09
	R^2	0.9998
Pseudo-first order	q_e (mg/g)	80.08
	K_1 $(\frac{1}{min})$	0.42
	R^2	0.986
Pseudo-second order	K_2 (g/mg.min)	0.0137
	q_e (mg/g)	82.01
	R^2	0.995

[44]. Hashemzadeh et al. reported a k_{id} value of 2.84 g/min$^{0.5}$.mg for AMX adsorption onto Av-N-AC, while in our study, the k_{id} was 32.01 for the first stage and decreased to 0.41 g/min$^{0.5}$.mg at the end of the third stage [51]. Unlike the present study, in another study, the IPD kinetic model had two adsorption stages. This means that the IPD was not the only controlling stage of the process and other adsorption phenomena may also control the TC removal [40]. Removal of Levofloxacin with MWCNTs/CoFe$_2$O$_4$ is carried out at several stages from surface of adsorbent to the IPD [73].

3.8. Isotherm study

The study on the isotherms of adsorption was done on the equilibrium data in order to determine the adsorption capacity and the interactions between MA-PK and AMX [74]. So, six non-linear models of Temkin, Langmuir, Dubinin-Radushkevich, Hill, Redlich-Peterson, and Freundlich were used to analyze the experimental data under equilibrium conditions [50]. The adsorption capacity of different amounts of AMX onto the MA-PK is shown in Fig. 10. Fig. 11 shows the non-linear fits of the isotherm's models including Temkin, Langmuir, Dubinin-Radushkevich, Hill, Redlich-Peterson and Freundlich. Parameters for all of the six isotherms were calculated (Table 4). The adsorption process was better followed by the Hill model with a R^2 of 0.987 and a q_H of 719.07 mg/g. Also, q_{max} from Langmuir was 512.27 mg per g of MA-PK. The R_L values for irreversible adsorption, linear adsorption, optimal adsorption state, and undesirable adsorption are 0, 1, between 0 and 1, and higher than 1. According to the results, R_L was 0.06, indicating the desirable adsorption of AMX on the MA-PK. In the Freundlich equation, n and K_f are the adsorption constants. In this equation, n is the adsorption rate and the adsorption is desirable if $1 < n < 10$, and n less than 1 indicates weak adsorption [75]. In this study, n was 3.74 which showed good adsorption. Rafati et al. stated the removal of ibuprofen followed the Freundlich isotherm model with $R^2 = 0.9525$ [72]. In Redlich-Peterson model, the exponent g was between 0 and 1, and it tends to 1 (g = 0.813). So, the Redlich-Peterson isotherm works like Langmuir isotherm and R^2 of Redlich-Peterson was 0.984 as well [43]. The results of other isotherm constants and parameters are shown in Table 4. In the Jan Bednárek study, Redlich-Peterson was the best isotherm model for fluoroquinolones removal by activated carbon and q_m, Langmuir for norfloxacin was 404 mg/g. But, unlike our study, the Freundlich model better described the adsorption process compared to Langmuir [41]. Isotherm models including Temkin, Dubinin-Radushkevich, Langmuir and Freundlich were also studied by Kyzas et al. (2022). Similar to our study, all of the models fitted to the experimental data with good R^2 values.

3.9. AMX removal from real hospital wastewater

To evaluate the absorbent efficiency of AMX removal, samples were prepared before the chlorination unit from a hospital in Bandar Abbas and filtered by 0.45 μm filters. Regarding Fig. 12, a chromatogram obtained from the spiked wastewater can be seen. It is observed that the AMX peak is separated from the wastewater samples. According to Table 5, good adsorbent efficiency for AMX removal is shown in the actual samples of hospital wastewater, which shows good adsorption performance.
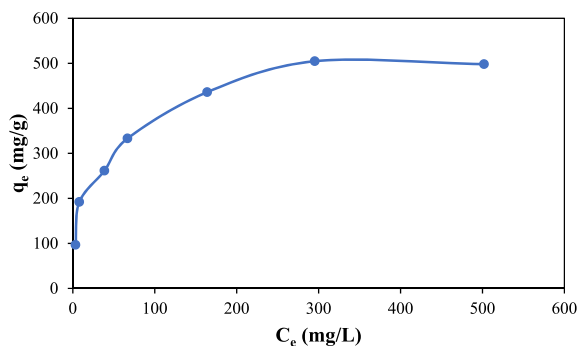

Fig. 10. The adsorption capacity of different amount of AMX onto the MA-PK (time = 60 min, pH = 5, C_{AMX} = 100–1000 mg/L, adsorbent dose = 1 g/L, rpm = 250).
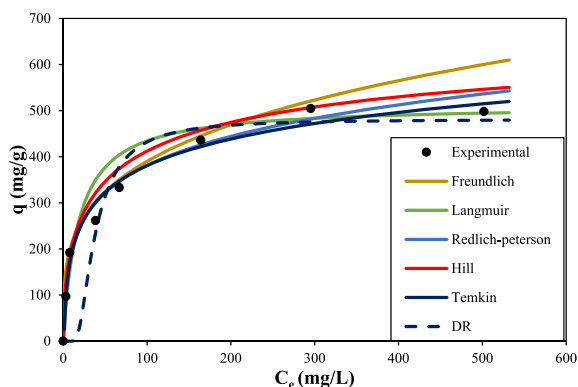

Fig. 11. The non-linear model of the adsorption isotherms.

Table 4

Parameters of the Langmuir, Freundlich, Hill, Dubinin-Radushkevich, Redlich-Peterson and Temkin isotherm models for AMX uptake onto the MA-PK.

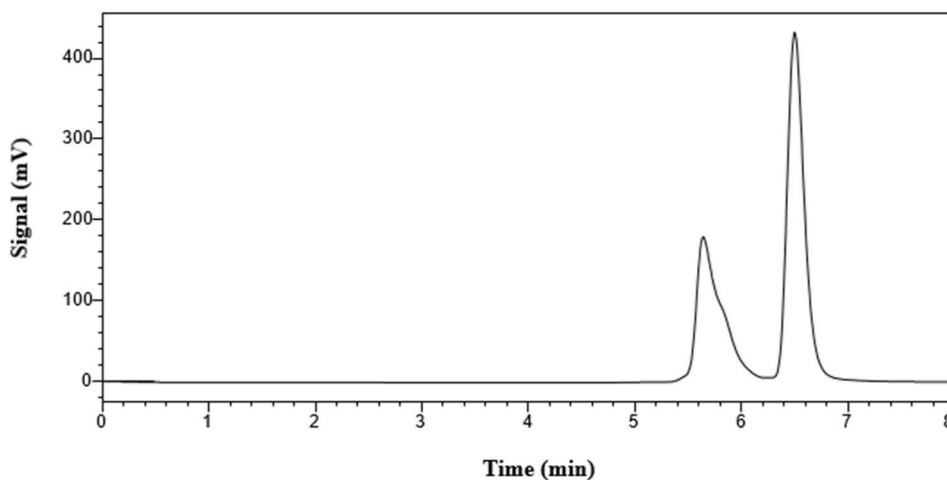| Isotherm models		pH = 5
Hill	$q_{H \, (mg/g)}$	719.07
	K_H	10.377
	n	0.531
	R^2	0.987
Temkin	K_T (L/g)	0.969
	b_T (J/mol)	29.76
	R^2	0.984
	R	8.314
	T (°K)	298
Freundlich	n_f	3.74
	K_F (mg/g)	103.48
	R^2	0.972
Langmuir	K_L (L/mg)	0.039
	q_{max} (mg/g)	512.27
	R^2	0.953
Redlich-Peterson	a_{RP} (L/mg)	66.22
	b_{RP} (L/g)	0.394
	g	0.813
	R^2	0.984
Dubinin-Radushkevich	q_{max} (mg/g)	481.25
	β	1.78
	R^2	0.792

Fig. 12. Hospital wastewater treatment for AMX uptake (time = 60 min, pH = 5, C_{AMX} = 400 mg/L, adsorbent dose = 1 g/L, rpm = 250).

Table 5

The results of AMX removal in the wastewater samples.

Sample	AMX Added (mg/L)	%R ± SD[a]
Hospital wastewater	–	Not detected
	300	86.89 ± 2.35
	400	83.05 ± 0.30
	600	75.51 ± 0.43

[a] Recovery percent plus standard deviation (n = 3).

3.10. Comparison studies

The capability of the prepared carbon-based adsorbent in the adsorption of AMX was compared with other studies. According to Table 6, the prepared AC in this research has an adsorption capacity as high as q_H = 719.07 and 512.27 mg/g from Hill and Langmuir isotherms, respectively, at a reaction time of 60 min. Also, due to good efficiency in the AMX removal from wastewater and water samples, which are the strength of this study, the AC-PK showed advantages over other adsorbents in the previous studies. Adsorption capacity presented by this work is superior or comparable to other works as well.

Table 6

Comparison of MA-PK with other carbon-based adsorbents in the adsorption of antibiotics from aqueous solutions.

Adsorbent	q_{max} (mg/g)	Time (min)	pH	Sample	Reference
Walnut shell based activated carbon	107.4 for Metronidazole and 93.5 for Sulfamethoxazole	2880	6	Aqueous solutions	[76]
Magnetic activated carbon	136.98	90	5	Aqueous solutions	[29]
Novel Chicken Feather Carbon	142.8571	5–7	<5	Aqueous solutions	[77]
Self-shaping porous biomass carbon foam pellets	64.23 for MNZ 82.58 for DMZ	120	4	Aqueous solutions	[78]
Activated carbon	4.4	240	5.5	Aqueous solutions	[79]
Activated carbon	424	300	4	Aqueous solutions	[80]
Magnetic activated olive kernel	238.1	90	6	Hospital wastewater	[35]
MA-PK	$q_{H,\ Hill}$ = 719.07 $q_{max,\ Langmuir}$ = 512.27	60	5	Hospital wastewater	This study

3.11. ANN modeling of AMX removal

In order to model the MA-PK adsorption, optimized ANN by input [8], hidden [29] and output [2] layers were used (Fig. 13). The optimized ANN topology biases and weights (w) that applied in this study is shown in Fig. 14. Also, Fig. 15 shows the agreement between experimental data of AMX removal and the predicted ANN model for the test sets. The plot of the test set has a correlation coefficient (0.979). According to the results, the model of ANN is a good method in order to predict the experimental data into the agreement ranges. So, the relative importance of the input factors to the efficiency of AMX adsorption (%) was calculated. Comparison between experimental and predicated data including key factors which affected the analysis results, is determined in Fig. 16. As for Fig. 17, the relative importance of AMX amount, MA-PK dose, pH, NaCl amount, and reaction time on the efficiency of AMX adsorption
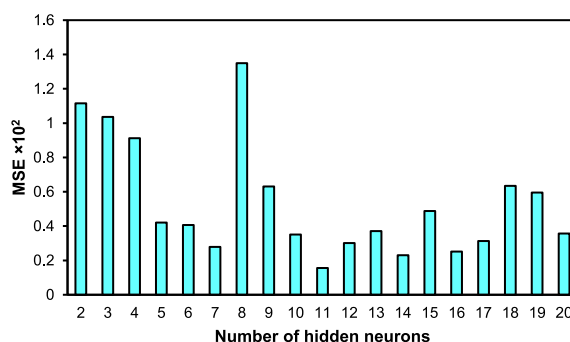

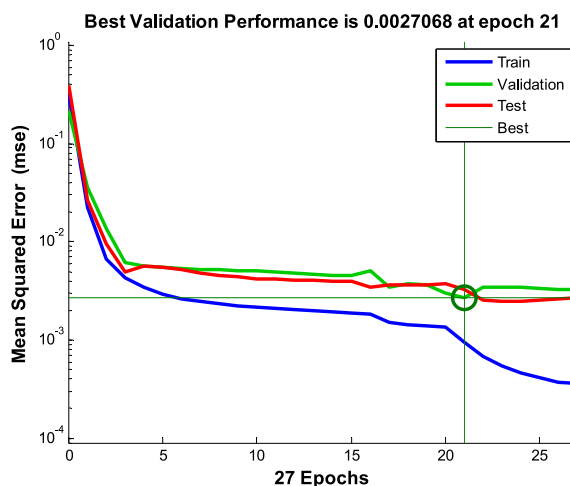**Fig. 13.** Performance of ANN as a function of neurons number.

Fig. 14. MSE progress with the number of iterations of training, validation, and test.
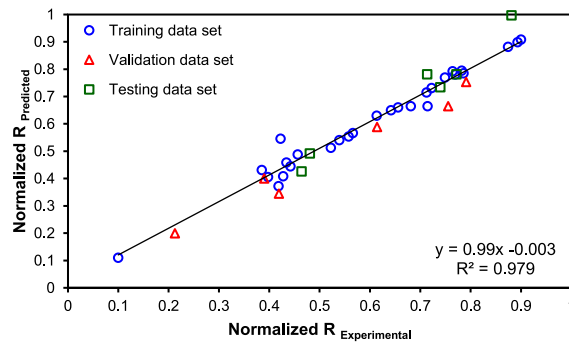
Fig. 15. Comparison of the normalized experimental results of DR89 removal efficiency with ANN predicted for the data set.
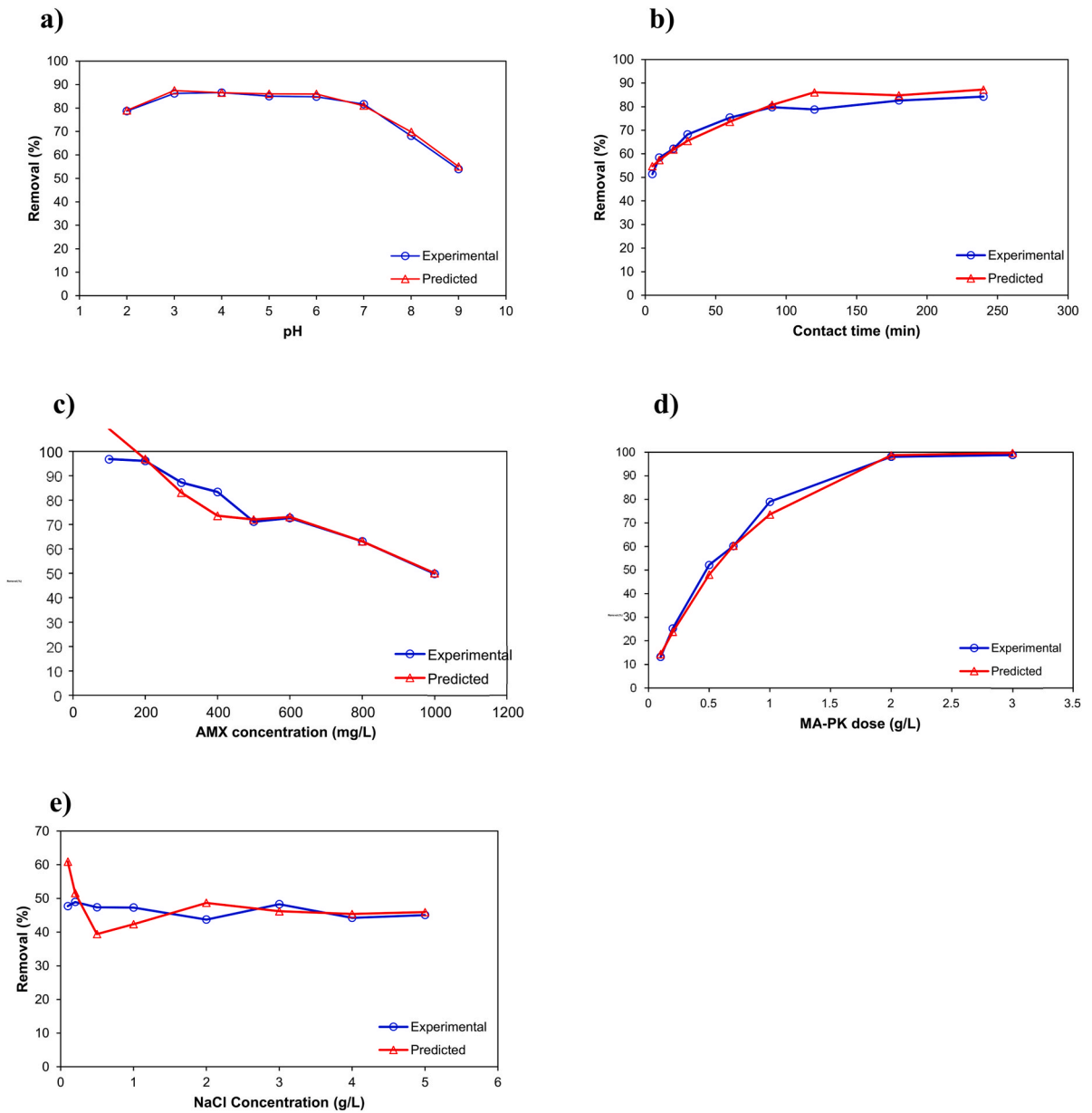

Fig. 16. Comparison between ANN predicted and experimental values of AMX removal as a function of (a) pH, (b) contact time, (c) AMX concentration, (d) MA-PK dose, and (e) NaCl concentration.
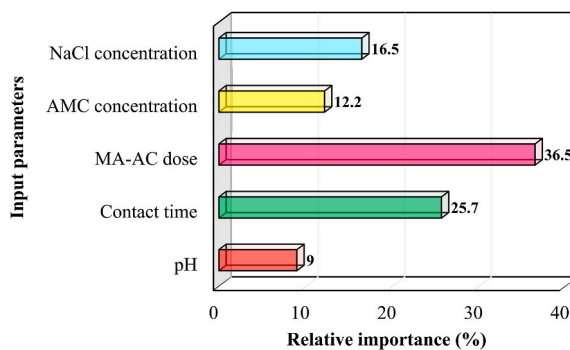
14

Fig. 17. The relative importance of input parameters on AMX removal efficiency.

was 12.2, 36.5, 9, 16.5 and 25.7%, respectively. Results by Ahmed F. Belhaj et al. have shown that the adopted model of ANN had good agreement with the data from the experimental condition that was similar to our results. Also, ANN utilization for such a prediction procedure can decrease the experimental reaction time, give practical predictions and operating cost rather than other computational processes [57]. In the Dalhat et al. study (2021), ANN modeling showed better predictions and bed depth < time < flow rate < initial concentration had the most influence on the phenol uptake, respectively [59]. Tanzifi et al. used the ANN molding with 5 input and 1 output, which was carried out by a hidden layer of 8 neurons. According to their results, ANN can calculate the methyl orange (MO) adsorption on the adsorbent (polyaniline) under different conditions [53].

4. Conclusion

In this study, lignin obtained from the PK was used as the basic compound for the preparation of adsorbent. Using an ultrasonic method, Fe_3O_4 magnetic particles were loaded on the surface of activated carbon-PK. Some methods were applied to determine and confirm the characteristics of the adsorbent such as FESEM, BET, XRD and FTIR analyses. The prepared final absorbent, with a good surface area (1852.4 m^2/g) confirmed using the BET test, was used to remove the AMX from hospital wastewater and aqueous solution. The six isotherms of Freundlich, Temkin, Redlich-Peterson, Dubinin-Radushkevich, Hill and Langmuir were studied in this study, which showed that Hill isotherm model was the best model. For kinetic study, four models, including pseudo-first-order, pseudo-second order, Elovich, and IPD were evaluated and data displays that the adsorption of AMX follows the Elovich model. According to ANN analysis, MA-PK concentration and reaction time had relative importance for AMX removal. Additionally, the adsorbent has shown high efficiency for AMX removal from a real matrix, hospital wastewater. Therefore, the MA-PK could be considered as an environmentally friendly, promising and efficient adsorbent for the removal of pharmaceuticals from wastewater solution. It is notable, the lack of access to advanced equipment and techniques such as the TEM is one of the limitations of the present study.

Author contribution statement

Khadijeh Jafari, Ali Fatehizadeh: Performed the experiments; Analyzed and interpreted the data; Wrote the paper.
Mohsen Heidari: Conceived and designed the experiments; Analyzed and interpreted the data; Wrote the paper.
Kavoos Dindarloo, Vali Alipour: Contributed reagents, materials, analysis tools or data; Wrote the paper.
Omid Rahmanian: Conceived and designed the experiments; Analyzed and interpreted the data; Contributed reagents, materials, analysis tools or data; Wrote the paper.

Data availability statement

Data will be made available on request.
Declaration of interest's statement:
The authors declare that they have no known competing financial interests or personal
relationships that could have appeared to influence the work reported in this paper.

Declaration of competing interest

The authors declare that they have no known competing financial interests or personal relationships that could have appeared to influence the work reported in this paper.

Acknowledgments

References

[1] I. Ali, S. Afshinb, Y. Poureshgh, A. Azari, Y. Rashtbari, A. Feizizadeh, et al., Green preparation of activated carbon from pomegranate peel coated with zero-valent iron nanoparticles (nZVI) and isotherm and kinetic studies of amoxicillin removal in water, Environ. Sci. Pollut. Res. 27 (2020) 36732–36743.

[2] P. Verlicchi, A. Galletti, M. Petrovic, D. Barceló, Hospital effluents as a source of emerging pollutants: an overview of micropollutants and sustainable treatment options, J. Hydrol. 389 (2010) 416–428.

[3] I.C. Vasilachi, D.M. Asiminicesei, D.I. Fertu, M. Gavrilescu, Occurrence and fate of emerging pollutants in water environment and options for their removal, Water 13 (2021) 181.

[4] G. Moussavi, A. Alahabadi, K. Yaghmaeian, M. Eskandari, Preparation, characterization and adsorption potential of the NH_4Cl-induced activated carbon for the removal of amoxicillin antibiotic from water, Chem. Eng. J. 217 (2013) 119–128.

[5] M. Ghoochian, H.A. Panahi, S. Sobhanardakani, L. Taghavi, A.H. Hassani, Synthesis and application of Fe_3O_4/SiO_2/thermosensitive/PAMAM-CS nanoparticles as a novel adsorbent for removal of tamoxifen from water samples, Microchem. J. 145 (2019) 1231–1240.

[6] D. Balarak, A. Joghatayi, F.K. Mostafapour, H. Azarpira, Biosorption of amoxicillin from contaminated water onto palm bark biomass, Int. J. Life Sci. Pharma Res. 7 (2017). L-9-L-16.

[7] A. Hrioua, A. Loudiki, A. Farahi, M. Bakasse, S. Lahrich, S. Saqrane, et al., Recent advances in electrochemical sensors for amoxicillin detection in biological and environmental samples, Bioelectrochemistry 137 (2021), 107687.

[8] D. Balarak, Y. Mahdavi, A. Maleki, H. Daraei, S. Sadeghi, Studies on the removal of amoxicillin by single walled carbon nanotubes, Br. J. Pharmaceut. Res. 10 (2016) 1.

[9] A.-S. Garnier, J. Dellamaggiore, B. Brilland, L. Lagarce, P. Abgueguen, A. Furber, et al., High incidence of amoxicillin-induced crystal nephropathy in patients receiving high dose of intravenous amoxicillin, J. Clin. Med. 9 (2020) 2022.

[10] M.R. Samarghandi, G. Asgari, R. Shokoohi, A. Dargahi, A. Arabkouhsar, Removing amoxicillin antibiotic from aqueous solutions by Saccharomyces cerevisiae bioadsorbent: kinetic, thermodynamic and isotherm studies, Desalination Water Treat. 152 (2019) 306–315.

[11] A.A. Aryee, R. Han, L. Qu, Occurrence, detection and removal of amoxicillin in wastewater: a review, J. Clean. Prod. 368 (2022), 133140.

[12] Ö. Kerkez-Kuyumcu, Ş.S. Bayazit, M.A. Salam, Antibiotic amoxicillin removal from aqueous solution using magnetically modified graphene nanoplatelets, J. Ind. Eng. Chem. 36 (2016) 198–205.

[13] M. Pirsaheb, H. Hossaini, N.K. Raad, S. Kianpour, H. Hossini, A systematic review on photo-fenton process as an efficient advanced oxidation for degradation of amoxicillin in aqueous environments, Rev. Environ. Health 38 (2023) 313–326.

[14] Y. Belaissa, D. Nibou, A. Assadi, B. Bellal, M. Trari, A new hetero-junction p-CuO/n-ZnO for the removal of amoxicillin by photocatalysis under solar irradiation, J. Taiwan Inst. Chem. Eng. 68 (2016) 254–265.

[15] H. Chakhtouna, H. Benzeid, N. Zari, R. Bouhfid, Functional $CoFe_2O_4$-modified biochar derived from banana pseudostem as an efficient adsorbent for the removal of amoxicillin from water, Sep. Purif. Technol. 266 (2021), 118592.

[16] B. Gao, J. Wang, M. Dou, C. Xu, X. Huang, Enhanced photocatalytic removal of amoxicillin with Ag/TiO_2/mesoporous gC_3N_4 under visible light: property and mechanistic studies, Environ. Sci. Pollut. Res. 27 (2020) 7025–7039.

[17] V. Homem, L. Santos, Degradation and removal methods of antibiotics from aqueous matrices–a review, J. Environ. Manag. 92 (2011) 2304–2347.

[18] Y.-L. Lin, C.-C. Tsai, N.-Y. Zheng, Improving the organic and biological fouling resistance and removal of pharmaceutical and personal care products through nanofiltration by using in situ radical graft polymerization, Sci. Total Environ. 635 (2018) 543–550.

[19] D. Nasuhoglu, A. Rodayan, D. Berk, V. Yargeau, Removal of the antibiotic levofloxacin (LEVO) in water by ozonation and TiO_2 photocatalysis, Chem. Eng. J. 189 (2012) 41–48.

[20] T. Saitoh, K. Shibata, M. Hiraide, Rapid removal and photodegradation of tetracycline in water by surfactant-assisted coagulation–sedimentation method, J. Environ. Chem. Eng. 2 (2014) 1852–1858.

[21] Z. Song, Y.-L. Ma, C.-E. Li, The residual tetracycline in pharmaceutical wastewater was effectively removed by using MnO_2/graphene nanocomposite, Sci. Total Environ. 651 (2019) 580–590.

[22] M. Klavarioti, D. Mantzavinos, D. Kassinos, Removal of residual pharmaceuticals from aqueous systems by advanced oxidation processes, Environ. Int. 35 (2009) 402–417.

[23] M. Shakak, R. Rezaee, A. Maleki, A. Jafari, M. Safari, B. Shahmoradi, et al., Synthesis and characterization of nanocomposite ultrafiltration membrane (PSF/PVP/SiO_2) and performance evaluation for the removal of amoxicillin from aqueous solutions, Environ. Technol. Innov. 17 (2020), 100529.

[24] S. Khan, M. Naushad, M. Govarthanan, J. Iqbal, S.M. Alfadul, Emerging contaminants of high concern for the environment: current trends and future research, Environ. Res. 207 (2022), 112609.

[25] S.-H. Lin, R.-S. Juang, Adsorption of phenol and its derivatives from water using synthetic resins and low-cost natural adsorbents: a review, J. Environ. Manag. 90 (2009) 1336–1349.

[26] R. Zandipak, S. Sobhanardakani, Novel mesoporous Fe_3O_4/SiO_2/CTAB–SiO_2 as an effective adsorbent for the removal of amoxicillin and tetracycline from water, Clean Technol. Environ. Policy 20 (2018) 871–885.

[27] A.O. Oluwole, E.O. Omotola, O.S. Olatunji, Pharmaceuticals and personal care products in water and wastewater: a review of treatment processes and use of photocatalyst immobilized on functionalized carbon in AOP degradation, BMC Chem 14 (2020) 1–29.

[28] S. Moosavi, C.W. Lai, S. Gan, G. Zamiri, O. Akbarzadeh Pivehzhani, M.R. Johan, Application of efficient magnetic particles and activated carbon for dye removal from wastewater, ACS Omega 5 (2020) 20684–20697.

[29] B. Kakavandi, A. Esrafili, A. Mohseni-Bandpi, A. Jonidi Jafari, R. Rezaei Kalantary, Magnetic Fe_3O_4@C nanoparticles as adsorbents for removal of amoxicillin from aqueous solution, Water Sci. Technol. 69 (2014) 147–155.

[30] K. Azam, N. Shezad, I. Shafiq, P. Akhter, F. Akhtar, F. Jamil, et al., A review on activated carbon modifications for the treatment of wastewater containing anionic dyes, Chemosphere 306 (2022), 135566.

[31] K. Khaledi, G.V. Labrada, J. Soltan, B. Predicala, M. Nemati, Adsorptive removal of tetracycline and lincomycin from contaminated water using magnetized activated carbon, J. Environ. Chem. Eng. 9 (2021), 105998.

[32] N. Dasgupta, S. Ranjan, C. Ramalingam, Applications of nanotechnology in agriculture and water quality management, Environ. Chem. Lett. 15 (2017) 591–605.

[33] H. Dong, Z. Jiang, C. Zhang, J. Deng, K. Hou, Y. Cheng, et al., Removal of tetracycline by Fe/Ni bimetallic nanoparticles in aqueous solution, J. Colloid Interface Sci. 513 (2018) 117–125.

[34] R. Soni, A.K. Pal, P. Tripathi, J.A. Lal, K. Kesari, V. Tripathi, An overview of nanoscale materials on the removal of wastewater contaminants, Appl. Water Sci. 10 (2020) 189.

[35] K. Jafari, M. Heidari, O. Rahmanian, Wastewater treatment for Amoxicillin removal using magnetic adsorbent synthesized by ultrasound process, Ultrason. Sonochem. 45 (2018) 248–256.

[36] A.L. Cazetta, A.M. Vargas, E.M. Nogami, M.H. Kunita, M.R. Guilherme, A.C. Martins, et al., NaOH-activated carbon of high surface area produced from coconut shell: kinetics and equilibrium studies from the methylene blue adsorption, Chem. Eng. J. 174 (2011) 117–125.

[37] A.R. Bagheri, M. Ghaedi, A. Asfaram, A.A. Bazrafshan, R. Jannesar, Comparative study on ultrasonic assisted adsorption of dyes from single system onto Fe_3O_4 magnetite nanoparticles loaded on activated carbon: experimental design methodology, Ultrason. Sonochem. 34 (2017) 294–304.

[38] T.A. Saleh, M. Tuzen, A. Sarı, Polyethylenimine modified activated carbon as novel magnetic adsorbent for the removal of uranium from aqueous solution, Chem. Eng. Res. Des. 117 (2017) 218–227.

[39] E.D. Revellame, D.L. Fortela, W. Sharp, R. Hernandez, M.E. Zappi, Adsorption kinetic modeling using pseudo-first order and pseudo-second order rate laws: a review, Clean. Eng. Technol. 1 (2020) 100032.

[40] J. Zhou, F. Ma, H. Guo, Adsorption behavior of tetracycline from aqueous solution on ferroferric oxide nanoparticles assisted powdered activated carbon, Chem. Eng. J. 384 (2020), 123290.

[41] J. Bednárek, L. Matějová, I. Koutník, M. Vráblová, G.J.F. Cruz, T. Strašák, et al., Revelation of high-adsorption-performance activated carbon for removal of fluoroquinolone antibiotics from water, Biomass Convers. Biorefin. (2022) 1–15.

[42] Z. Heidarinejad, O. Rahmanian, M. Fazlzadeh, M. Heidari, Enhancement of methylene blue adsorption onto activated carbon prepared from Date Press Cake by low frequency ultrasound, J. Mol. Liq. 264 (2018) 591–599.

[43] S. Norouzi, M. Heidari, V. Alipour, O. Rahmanian, M. Fazlzadeh, F. Mohammadi-Moghadam, et al., Preparation, characterization and Cr (VI) adsorption evaluation of NaOH-activated carbon produced from Date Press Cake; an agro-industrial waste, Bioresour. Technol. 258 (2018) 48–56.

[44] G.Z. Kyzas, G. McKay, T.J. Al-Musawi, S. Salehi, D. Balarak, Removal of benzene and toluene from synthetic wastewater by adsorption onto magnetic zeolitic imidazole framework nanocomposites, Nanomaterials 12 (2022) 3049.

[45] J. Yang, S. Shojaei, S. Shojaei, Removal of drug and dye from aqueous solutions by graphene oxide: adsorption studies and chemometrics methods, NPJ Clean Water 5 (2022) 5.

[46] M.H. Dehghani, D. Sanaei, I. Ali, A. Bhatnagar, Removal of chromium (VI) from aqueous solution using treated waste newspaper as a low-cost adsorbent: kinetic modeling and isotherm studies, J. Mol. Liq. 215 (2016) 671–679.

[47] Ç. Sarici-Özdemir, Y. Önal, Study to observe the applicability of the adsorption isotherms used for the adsorption of medicine organics onto activated carbon, Part. Sci. Technol. 36 (2018) 254–261.

[48] R. Khosravi, G. Moussavi, M.T. Ghaneian, M.H. Ehrampoush, B. Barikbin, A.A. Ebrahimi, et al., Chromium adsorption from aqueous solution using novel green nanocomposite: adsorbent characterization, isotherm, kinetic and thermodynamic investigation, J. Mol. Liq. 256 (2018) 163–174.

[49] F. Kord Mostafapour, R. Zolghadr, M. Khodadadi Saloot, A.H. Mahvi, D. Balarak, E. Safari, Removal of Acid blue 113 from aqueous medium using a novel magnetic adsorbent derived from activated carbon fiber, Int. J. Environ. Anal. Chem. (2022) 1–16.

[50] T.J. Al-Musawi, G. McKay, A. Kadhim, M.M. Joybari, D. Balarak, Activated carbon prepared from hazelnut shell waste and magnetized by Fe_3O_4 nanoparticles for highly efficient adsorption of fluoride, Biomass Convers. Biorefin. (2022) 1–16.

[51] F. Hashemzadeh, M. Ariannezhad, S.H. Derakhshandeh, Evaluation of Cephalexin and Amoxicillin removal from aqueous media using activated carbon produced from Aloe vera leaf waste, Chem. Phys. Lett. 800 (2022), 139656.

[52] Y. Khaksarfard, A. Bagheri, A.A. Rafati, Synergistic effects of binary surfactant mixtures in the adsorption of diclofenac sodium drug from aqueous solution by modified zeolite, J. Colloid Interface Sci. 644 (2023) 186–199.

[53] M. Tanzifi, S.H. Hosseini, A.D. Kiadehi, M. Olazar, K. Karimipour, R. Rezaiemehr, et al., Artificial neural network optimization for methyl orange adsorption onto polyaniline nano-adsorbent: kinetic, isotherm and thermodynamic studies, J. Mol. Liq. 244 (2017) 189–200.

[54] N.G. Turan, B. Mesci, O. Ozgonenel, The use of artificial neural networks (ANN) for modeling of adsorption of Cu (II) from industrial leachate by pumice, Chem. Eng. J. 171 (2011) 1091–1097.

[55] A.A. Babaei, A. Khataee, E. Ahmadpour, M. Sheydaei, B. Kakavandi, Z. Alaee, Optimization of cationic dye adsorption on activated spent tea: equilibrium, kinetics, thermodynamic and artificial neural network modeling, Kor. J. Chem. Eng. 33 (2016) 1352–1361.

[56] S. Dutta, S.A. Parsons, C. Bhattacharjee, S. Bandhyopadhyay, S. Datta, Development of an artificial neural network model for adsorption and photocatalysis of reactive dye on TiO_2 surface, Expert Syst. Appl. 37 (2010) 8634–8638.

[57] A.F. Belhaj, K.A. Elraies, M.S. Alnarabiji, F.A.A. Kareem, J.A. Shuhli, S.M. Mahmood, et al., Experimental investigation, binary modelling and artificial neural network prediction of surfactant adsorption for enhanced oil recovery application, Chem. Eng. J. 406 (2021), 127081.

[58] M. Yusuf, K. Song, L. Li, Fixed bed column and artificial neural network model to predict heavy metals adsorption dynamic on surfactant decorated graphene, Colloids Surf. A Physicochem. Eng. Asp. 585 (2020), 124076.

[59] M.A. Dalhat, N.D. Mu'Azu, M.H. Essa, Generalized decay and artificial neural network models for fixed-Bed phenolic compounds adsorption onto activated date palm biochar, J. Environ. Chem. Eng. 9 (2021).

[60] A.M. Ghaedi, A. Vafaei, Applications of artificial neural networks for adsorption removal of dyes from aqueous solution: a review, Adv. Colloid Interface Sci. 245 (2017) 20–39.

[61] O. Filippou, E.A. Deliyanni, V.F. Samanidou, Fabrication and evaluation of magnetic activated carbon as adsorbent for ultrasonic assisted magnetic solid phase dispersive extraction of bisphenol A from milk prior to high performance liquid chromatographic analysis with ultraviolet detection, J. Chromatogr. A 1479 (2017) 20–31.

[62] E.K. Faulconer, N.V.H. von Reitzenstein, D.W. Mazyck, Optimization of magnetic powdered activated carbon for aqueous Hg (II) removal and magnetic recovery, J. Hazard Mater. 199 (2012) 9–14.

[63] O. Pezoti, A.L. Cazetta, K.C. Bedin, L.S. Souza, A.C. Martins, T.L. Silva, et al., NaOH-activated carbon of high surface area produced from guava seeds as a high-efficiency adsorbent for amoxicillin removal: kinetic, isotherm and thermodynamic studies, Chem. Eng. J. 288 (2016) 778–788.

[64] D. Shan, S. Deng, T. Zhao, B. Wang, Y. Wang, J. Huang, et al., Preparation of ultrafine magnetic biochar and activated carbon for pharmaceutical adsorption and subsequent degradation by ball milling, J. Hazard Mater. 305 (2016) 156–163.

[65] A. Kumar, H.M. Jena, Adsorption of Cr (VI) from aqueous solution by prepared high surface area activated carbon from Fox nutshell by chemical activation with H_3PO_4, J. Environ. Chem. Eng. 5 (2017) 2032–2041.

[66] I.H. Alsohaimi, M.A. Khan, Z.A. Alothman, M.R. Khan, M. Kumar, Synthesis, characterization, and application of Fe-CNTs nanocomposite for BrO_3- remediation from water samples, J. Ind. Eng. Chem. 26 (2015) 218–225.

[67] E. Sharifpour, H.Z. Khafri, M. Ghaedi, A. Asfaram, R. Jannesar, Isotherms and kinetic study of ultrasound-assisted adsorption of malachite green and Pb^{2+} ions from aqueous samples by copper sulfide nanorods loaded on activated carbon: experimental design optimization, Ultrason. Sonochem. 40 (2018) 373–382.

[68] V. Hasanzadeh, O. Rahmanian, M. Heidari, Cefixime adsorption onto activated carbon prepared by dry thermochemical activation of date fruit residues, Microchem. J. 152 (2020), 104261.

[69] Y. Zhang, C. Zhu, F. Liu, Y. Yuan, H. Wu, A. Li, Effects of ionic strength on removal of toxic pollutants from aqueous media with multifarious adsorbents: a review, Sci. Total Environ. 646 (2019) 265–279.

[70] M.R. Samarghandi, T.J. Al-Musawi, A. Mohseni-Bandpi, M. Zarrabi, Adsorption of cephalexin from aqueous solution using natural zeolite and zeolite coated with manganese oxide nanoparticles, J. Mol. Liq. 211 (2015) 431–441.

[71] Y. Tong, P.J. McNamara, B.K. Mayer, Adsorption of organic micropollutants onto biochar: a review of relevant kinetics, mechanisms and equilibrium, Environ. Sci. Water Res. Technol. 5 (2019) 821–838.

[72] L. Rafati, M. Ehrampoush, A. Rafati, M. Mokhtari, A. Mahvi, Removal of ibuprofen from aqueous solution by functionalized strong nano-clay composite adsorbent: kinetic and equilibrium isotherm studies, Int. J. Environ. Sci. Technol. 15 (2018) 513–524.

[73] T.J. Al-Musawi, Y.Q. Almajidi, E.M. Al-Essa, R.M. Romero-Parra, E.R. Alwaily, N. Mengelizadeh, et al., Levofloxacin adsorption onto $MWCNTs/CoFe_2O_4$ nanocomposites: mechanism, and modeling using non-linear kinetics and isotherm equations, Magnetochemistry 9 (2023) 9.

[74] J. Wang, X. Guo, Adsorption isotherm models: classification, physical meaning, application and solving method, Chemosphere 258 (2020), 127279.

[75] A.R. Agcaoili, M.U. Herrera, C.M. Futalan, M.D.L. Balela, Fabrication of polyacrylonitrile-coated kapok hollow microtubes for adsorption of methyl orange and Cu (II) ions in aqueous solution, J. Taiwan Inst. Chem. Eng. 78 (2017) 359–369.

[76] S. Teixeira, C. Delerue-Matos, L. Santos, Application of experimental design methodology to optimize antibiotics removal by walnut shell based activated carbon, Sci. Total Environ. 646 (2019) 168–176.

[77] H. Li, J. Hu, C. Wang, X. Wang, Removal of amoxicillin in aqueous solution by a novel chicken feather carbon: kinetic and equilibrium studies, Water Air Soil Pollut. 228 (2017) 1–13.

[78] L. Sun, S. Wan, D. Yuan, Z. Yu, Adsorption of nitroimidazole antibiotics from aqueous solutions on self-shaping porous biomass carbon foam pellets derived from Vallisneria natans waste as a new adsorbent, Sci. Total Environ. 664 (2019) 24–36.

[79] M.A.E. de Franco, C.B. de Carvalho, M.M. Bonetto, R. de Pelegrini Soares, L.A. Féris, Removal of amoxicillin from water by adsorption onto activated carbon in batch process and fixed bed column: kinetics, isotherms, experimental design and breakthrough curves modelling, J. Clean. Prod. 161 (2017) 947–956.

[80] M. Belhachemi, S. Djelaila, Removal of amoxicillin antibiotic from aqueous solutions by date pits activated carbons, Environ. Process. 4 (2017) 549–561.